


IABSE Task Group 3.1 Benchmark Results. Part 2: Numerical Analysis of a Three-Degree-of-Freedom Bridge Deck Section Based on Experimental Aerodynamics

Giorgio Diana Chair of Task Group 3.1, Stoyan Stoyanoff Vice-Chair of Task Group 3.1, Dr Ketil Aas-Jakobsen, Dr Andrew Allsop, Dr Michael Andersen, Dr Tommaso Argentini, Dr Miguel Cid Montoya, Santiago Hernández (Prof.), José Ángel Jurado (Prof.), Hiroshi Katsuchi (Prof.), Dr Igor Kavrov, Ho-Kyung Kim(Prof.), Guy Larose, Dr Allan Larsen, Guido Morgenthal (Prof.), Ole Øiseth (Prof.), Dr Simone Omarini, Daniele Rocchi(Prof.), Dr Martin Svendsen & Teng Wu (Prof.)

To cite this article: Giorgio Diana Chair of Task Group 3.1, Stoyan Stoyanoff Vice-Chair of Task Group 3.1, Dr Ketil Aas-Jakobsen, Dr Andrew Allsop, Dr Michael Andersen, Dr Tommaso Argentini, Dr Miguel Cid Montoya, Santiago Hernández (Prof.), José Ángel Jurado (Prof.), Hiroshi Katsuchi (Prof.), Dr Igor Kavrov, Ho-Kyung Kim(Prof.), Guy Larose, Dr Allan Larsen, Guido Morgenthal (Prof.), Ole Øiseth (Prof.), Dr Simone Omarini, Daniele Rocchi(Prof.), Dr Martin Svendsen & Teng Wu (Prof.) (2019): IABSE Task Group 3.1 Benchmark Results. Part 2: Numerical Analysis of a Three-Degree-of-Freedom Bridge Deck Section Based on Experimental Aerodynamics, Structural Engineering International, DOI: [10.1080/10168664.2019.1661331](https://doi.org/10.1080/10168664.2019.1661331)

To link to this article: <https://doi.org/10.1080/10168664.2019.1661331>

 View supplementary material [↗](#)

 Published online: 15 Oct 2019.

 Submit your article to this journal [↗](#)

 Article views: 33

 View related articles [↗](#)

 View Crossmark data [↗](#)

IABSE Task Group 3.1 Benchmark Results. Part 2: Numerical Analysis of a Three-Degree-of-Freedom Bridge Deck Section Based on Experimental Aerodynamics

Giorgio Diana, Chair of Task Group 3.1, Politecnico di Milano, Milan, Italy; **Stoyan Stoyanoff**, Vice-Chair of Task Group 3.1, RWDI, Guelph, ON, Canada; **Ketil Aas-Jakobsen**, Dr, Ing. A. Aas-Jakobsen AS, Oslo, Norway; **Andrew Allsop**, Dr, ARUP, London, UK; **Michael Andersen**, Dr, Svend Ole Hansen ApS, Odense, Denmark; **Tommaso Argentini** , Dr, Politecnico di Milano, Milan, Italy; **Miguel Cid Montoya** , Dr, University of A Coruña, A Coruña, Spain; **Santiago Hernández**, Prof., University of A Coruña, A Coruña, Spain; **José Ángel Jurado**, Prof., University of A Coruña, A Coruña, Spain; **Hiroshi Katsuchi**, Prof., Yokohama National University, Yokohama, Japan; **Igor Kavrakov**, Dr, Bauhaus-University Weimar, Weimar, Germany; **Ho-Kyung Kim** , Prof., Seoul National University, Seoul, Republic of Korea; **Guy Larose**, RWDI, Guelph, ON, Canada; **Allan Larsen**, Dr, COWI, Kongens Lyngby, Denmark; **Guido Morgenthal**, Prof., Bauhaus-University Weimar, Weimar, Germany; **Ole Øiseth**, Prof., Norwegian University of Science and Technology, Trondheim, Norway; **Simone Omarini**, Dr; **Daniele Rocchi** , Prof., Politecnico di Milano, Milan, Italy; **Martin Svendsen**, Dr, Ramboll, Copenhagen, Denmark; **Teng Wu**, Prof., University of Buffalo, Buffalo, NY, USA. Contact: tommaso.argentini@polimi.it. DOI: 10.1080/10168664.2019.1661331

Abstract

IABSE Task Group 3.1 has the mandate to define reference results for the validation of methodologies and programs used to study both stability and buffeting responses of long-span bridges. To this end, the working group set up a benchmark procedure consisting of several steps with increasing complexity to define reference results useful for this validation. The simplest step (1.1a) was presented in Part 1. In this paper (Part 2), the contributions and reference results of the second sub-step (1.1c) are discussed. It consists of the simulation of the aeroelastic response of a three-degree-of-freedom bridge deck section forced by turbulent wind, using experimental aerodynamic coefficients measured in a wind tunnel. The increase in complexity, compared to the previous step, involves the experimental definition of unsteady force coefficients that are defined in a limited range of reduced velocities, and inclusion of the lateral motion and horizontal turbulent wind velocity components. Comparison of the different outputs, obtained by Task Group 3.1 participants with the same input data, is presented, revealing differences that are not always negligible. Moreover, the increase in complexity of the test case results in larger spreads of the results compared to the fully analytical case, analysed in Part 1.

Keywords: Benchmark; aeroelasticity; flutter; buffeting; long-span bridge; validation

Introduction

The International Association for Bridge and Structural Engineering (IABSE) Task Group 3.1 (“Super-Long-Span Bridge Aerodynamics”) is developing a series of benchmark tests to define reference results for the validation of numerical methodologies and software programs for the assessment of the aeroelastic behaviour of long-span bridges exposed to wind action.

The benchmark consists of three principal steps (Steps 1, 2 and 3) with sub-steps of increasing complexity (see Ref. [1] for a complete description of the benchmark structure). Step 1 is a comparison of different numerical results, while Steps 2 and 3 will provide a comparison between

numerical and experimental results (wind tunnel tests and full-scale measurements, respectively).

At the end of the first year of activity, the dissemination of the output of Step 1 started. The results of the simplest benchmark tests (Step 1.1a) are discussed in the companion paper, “IABSE Task Group 3.1 benchmark results. Part 1: Numerical analysis of a two-degree-of-freedom bridge deck section based on analytical aerodynamics”,¹ while in this paper the results of the more complex Step 1.1c benchmark tests are presented.

Step 1.1a examined a basic aeroelastic problem: the stability and the buffeting response of a bridge deck section with two degrees of freedom (DOF): vertical and torsional. The Theodorsen

functions of a flat plate were used to analytically define aeroelastic forces over the entire range of reduced velocity. Only the vertical component w of wind turbulence was considered, with analytical admittance functions to compute buffeting forces, at 0 degree mean angle of attack only.

The new features studied in Step 1.1c with respect to the previous step (Step 1.1a) are:

1. Aerodynamic coefficients are not analytical, but experimentally measured through wind tunnel tests; in particular, they are defined in a limited range of reduced velocities, at 0 degree mean angle of attack only. This requires an interpolation/extrapolation of the values to be used in the numerical simulation.
2. Three degrees of freedom are considered instead of two, including the lateral motion.
3. Both the vertical and the horizontal components of turbulence, w and u , are considered in a single cross-section, keeping an analytical formulation for the buffeting forces.

Input data, provided to all Task Group (TG) contributors, are described in the subsection “Input for Step 1.1c Analysis”, and can be downloaded from the Supplemental Material of the present paper (on the website of *Structural Engineering International*). As an alternative, the same data can be downloaded from the IABSE website. The output results used in the benchmark are described in the subsection “Required Output for Step 1.1c” and the results are then compared in

Quantity	Description	Value
m_L [kg/m]	Mass per unit length	22 740
J_L [kg m ² /m]	Moment of inertia per unit length	2.47×10^6
B [m]	Deck chord	31
f_y [Hz]	Lateral eigenfrequency	0.052
f_z [Hz]	Vertical eigenfrequency	0.10
f_θ [Hz]	Torsional eigenfrequency	0.278
ξ [-]	Damping ratio (for all modes)	0.003

Table 1: Deck section model structural data

“Results of Step 1.1c”. Reference results and their statistical analysis are summarized in the section “Step 1.1c: Reference Values”; everyone can check their numerical codes using these data.

Benchmark: Step 1.1c

Input for Step 1.1c Analysis

The input data for the simulation of the deck aeroelastic response comprise:

- structural parameters of the bridge deck section
- turbulent wind characteristics
- aerodynamic coefficients.

Structural Parameters

Structural input data of the 3 DOF sectional model are reported in Table 1. The real full-scale values (mass per unit length, structural natural frequencies, damping ratio and deck chord) of the Storebælt bridge are used, to relate to real applications. Owing to limited coupling between the structural modes of the Storebælt bridge, the structural modes of the bridge deck

section in this analysis are considered uncoupled.

Turbulent Wind Characteristics

The mean wind speed U and the horizontal and the vertical components of turbulent wind (u and w , respectively) in a single point are considered in the simulation. Five mean wind speed scenarios are considered to compare the results with an increasing level of aerodynamic coupling up to a wind speed close to flutter instability. The characteristics of the simulated wind are reported in Table 2. Ten 600 s long time histories of the turbulent wind components were generated according to the Von Karman spectrum using a time-step of 0.05 s, to allow the use of time domain (TD) methods. A harmonic superposition method was used for the generation of the time histories.^{2,3} The time histories of $u(t)$ and $w(t)$ are available in the Supplemental Material. As shown in Table 2, the cross-power spectrum $S_{uw}(f)$ of the incoming turbulence is forced to be equal to zero, to consider a complete lack of correlation between wind velocity components.

The method used for wind generation was selected for convenience. The investigation of the wind field generation problem is not a task of the benchmark and is beyond the scope of this study.

Aerodynamic Forces

The standard approach used to model the aerodynamic forces is based on a linearized model of the fluid–structure interaction around a steady configuration of the bridge, which depends on the mean wind speed.

The aerodynamic forces (F_{aero}) acting on the deck can be modelled as the sum of three different components, namely:

- F_{st} , the steady aerodynamic forces
- F_{se} , the self-excited (or motion-induced) forces
- F_{buff} , the buffeting forces.

The steady aerodynamic forces F_{st} depend on the mean wind speed only, the self-excited forces F_{se} depend on bridge motion, and the buffeting forces F_{buff} depend on the incoming wind turbulence.

Using the sign conventions reported in Fig. 1, the steady aerodynamic drag (F_D), lift (F_L) and moment (M) per unit length acting on the deck section are defined through steady coefficients as functions of the angle of attack α :

$$F_{st} = \frac{1}{2} \rho U^2 B \begin{bmatrix} C_D(\alpha) \\ C_L(\alpha) \\ BC_M(\alpha) \end{bmatrix} \quad (1)$$

where B is the deck chord, U is the mean wind velocity, and ρ is the air density. C_D , C_L , C_M are, respectively, the drag, lift and moment static

Wind speeds	$U = 15, 30, 45, 60, 75$ m/s
Air density	$\rho = 1.22$ kg/m ³
Turbulence intensity [$\sigma_{u,w}$ is the standard deviation of $u(t)$, $w(t)$]	$I_u = \frac{\sigma_u}{U} = 0.10$ $I_w = \frac{\sigma_w}{U} = 0.05$
Integral length scale	${}^xL_u = 200$ m ${}^xL_w = 20$ m
Von Karman power spectrum of u and w , as a function of frequency f	$\frac{f \cdot S_u(f)}{\sigma_u^2} = \frac{4 \left(\frac{f^x L_u}{U} \right)}{\left[1 + 70.8 \left(\frac{f^x L_u}{U} \right)^2 \right]^{5/6}} \frac{f \cdot S_w(f)}{\sigma_w^2} = \frac{4 \left(\frac{f^x L_w}{U} \right) \left(1 + 755.2 \left(\frac{f^x L_w}{U} \right)^2 \right)}{\left[1 + 283.2 \left(\frac{f^x L_w}{U} \right)^2 \right]^{11/6}}$ $S_{uw}(f) = S_{wu}(f) = 0$

Table 2: Incoming wind characteristics

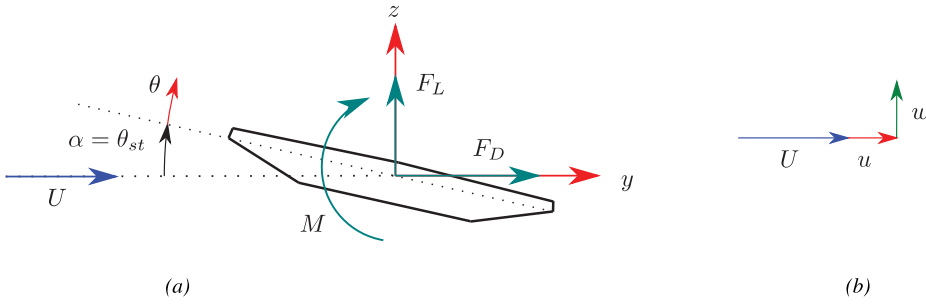


Fig. 1: Sign conventions: (a) deck forces and displacements; (b) turbulent wind

coefficients, measured through wind tunnel tests.

Self-excited forces F_{se} per unit length are defined through the flutter derivative coefficients using a linearized approach around the steady position of the bridge. Typically, flutter derivative coefficients are measured experimentally on rigid sectional models in wind tunnels for a discrete number of reduced velocities requiring an interpolation and/or extrapolation to simulate conditions where experimental data are not available.⁴ The Polimi formulation for flutter derivatives⁵ is used in this paper for convenience, since this notation is closer to the Theodorsen functions for a flat plate, used in the previous paper.¹

The coefficients in the classical Scanlan formulation are available in the Supplemental Material. Considering lateral, vertical and torsional harmonic motions around the steady position of the bridge, the self-excited forces per unit length F_{se} acting on the bridge deck are expressed through 18 flutter derivatives as:

$$F_{D,se} = \frac{1}{2} \rho U^2 B \left(-p_1^* \frac{\dot{z}}{U} - p_2^* \frac{B\dot{\theta}}{U} + p_3^* \theta + \frac{2\pi^3}{V^{*2}} p_4^* \frac{z}{B} - p_5^* \frac{\dot{y}}{U} + \frac{2\pi^3}{V^{*2}} p_6^* \frac{y}{B} \right) \quad (2)$$

$$F_{L,se} = \frac{1}{2} \rho U^2 B \left(-h_1^* \frac{\dot{z}}{U} - h_2^* \frac{B\dot{\theta}}{U} + h_3^* \theta + \frac{2\pi^3}{V^{*2}} h_4^* \frac{z}{B} - h_5^* \frac{\dot{y}}{U} + \frac{2\pi^3}{V^{*2}} h_6^* \frac{y}{B} \right) \quad (3)$$

$$M_{se} = \frac{1}{2} \rho U^2 B^2 \left(-a_1^* \frac{\dot{z}}{U} - a_2^* \frac{B\dot{\theta}}{U} + a_3^* \theta + \frac{2\pi^3}{V^{*2}} a_4^* \frac{z}{B} - a_5^* \frac{\dot{y}}{U} + \frac{2\pi^3}{V^{*2}} a_6^* \frac{y}{B} \right) \quad (4)$$

where p_i^* are the flutter derivatives for drag force $F_{D,se}$, h_i^* are the flutter derivatives for lift force $F_{L,se}$, and a_i^* are the flutter derivatives for the moment M_{se} . $V^* = U/(fB)$ is the reduced velocity, f being the frequency and B the deck chord. y , z and θ are, respectively, the lateral, vertical (positive upward) and torsional (positive nose-up) displacements of the sectional bridge around the static configuration (Fig. 1).

The experimental flutter derivatives of the Storebælt bridge deck measured in the wind tunnel are used.⁶ Coefficients are reported in Figs. 2–4, only for a 0 degree mean angle of attack, as a function of the reduced velocity. Only values in the range $5 < V^* < 35$ are available, for a discrete set of V^* every $\Delta V^* = 5$. Since the experimental flutter derivatives are available for a 0 degree mean angle of attack only, the static configuration of the bridge is supposed to be equal to zero.

The buffeting forces F_{buff} per unit length due to incoming turbulent wind u and w are defined in the

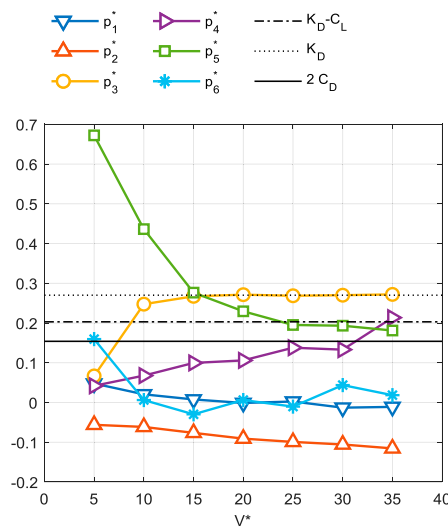


Fig. 2: Drag derivatives: Storebælt p^* values as a function of V^* , and quasi steady theory (QST) coefficients

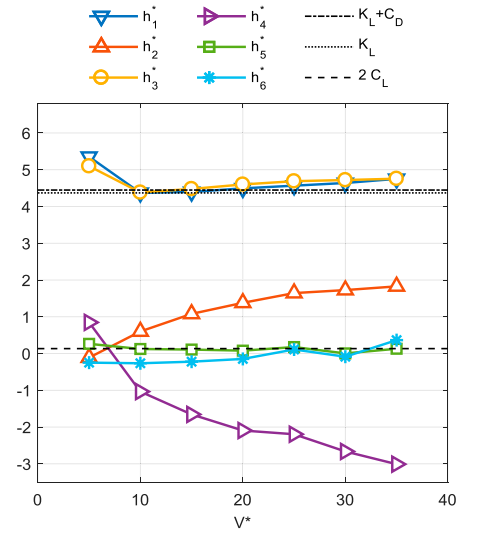


Fig. 3: Lift derivatives: Storebælt h^* values as a function of V^* , and quasi steady theory (QST) coefficients

frequency domain (FD) through the admittance functions:

$$\tilde{\mathcal{F}} \begin{Bmatrix} F_{D,buff} \\ F_{L,buff} \\ M_{buff} \end{Bmatrix} = \frac{1}{2} \rho U B \begin{bmatrix} \chi_{Du}^* & \chi_{Dw}^* \\ \chi_{Lu}^* & \chi_{Lw}^* \\ B\chi_{Mu}^* & B\chi_{Mw}^* \end{bmatrix} \tilde{\mathcal{F}} \begin{Bmatrix} u(t) \\ w(t) \end{Bmatrix} \quad (5)$$

where $\tilde{\mathcal{F}}$ is the Fourier transform operator; χ^* are called admittance functions and they depend upon the reduced velocity V^* and the mean angle of attack.

Typically, the admittance functions χ^* are measured as a function of the reduced velocity and the mean angle of attack through wind tunnel tests on sectional models, in a similar way to what is done for the flutter derivative coefficients.

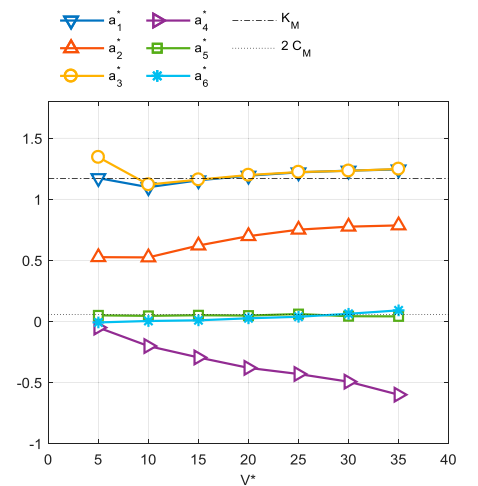


Fig. 4: Moment derivatives: Storebælt a^* values as a function of V^* , and quasi steady theory (QST) coefficients

The χ^* are defined using the quasi-steady values weighted by the Davenport function $A(V^*)$ as:

$$\begin{aligned}\chi_{Du}^* &= 2C_D A(V^*) = 0.154A(V^*) \\ \chi_{Lu}^* &= 2C_L A(V^*) = 0.134A(V^*) \\ \chi_{Mu}^* &= 2C_M A(V^*) = 0.056A(V^*) \\ \chi_{Dw}^* &= (K_D - C_L)A(V^*) = 0.203A(V^*) \\ \chi_{Lw}^* &= (K_L + C_D)A(V^*) = 4.447A(V^*) \\ \chi_{Mw}^* &= K_M A(V^*) = 1.17A(V^*)\end{aligned}\quad (6)$$

where $A(V^*)$ is a real weighting function in reduced velocity:

$$A(V^*) = \frac{2}{(7/V^*)^2} (7/V^* - 1 + e^{-7/V^*}) \quad (7)$$

This choice is made to obtain a function defined analytically over the complete range of V^* , as was done for Step 1.1a.¹

The main aim of the benchmark is to compare the dynamic response of the sectional bridge due to the self-excited F_{se} and buffeting forces F_{buff} around the steady configuration of the bridge, forcing the model with the stationary aerodynamic forces F_{st} only. The experimental flutter derivatives are available for 0 degree mean angle of attack only, and therefore the static configuration of the bridge is supposed to be equal to zero ($y_{st} = 0$, $z_{st} = 0$, $\theta_{st} = 0$).

Required Output for Step 1.1c

The following results were provided by the TG members:

1. Aeroelastic stability in smooth flow:
 - (a) critical flutter speed of the bridge
 - (b) frequency and damping ratio of the three vibration modes as functions of mean wind speed.
2. Buffeting response in turbulent flow:
 - (a) standard deviation (STD) of displacements y , z and θ as a function of mean wind speed
 - (b) comparison of power spectral densities (PSDs) of y , z and θ .

These results are presented and analysed in the following section, with the aim of selecting the most meaningful quantities for validating the numerical models and corresponding reference values.

Results of Step 1.1c

For this benchmark test, TG members used their own methodology and codes to simulate the bridge behaviour, starting from the same input data.^{5,7-28} All the results were then compared, and reference values were defined with statistical analysis.

Aeroelastic Stability in Smooth Flow

To define reference values, the same statistical procedure presented in Ref. [1] is applied for all results. In brief, the following strategy is applied to define a reference:

1. The mean μ^* and the standard deviation σ^* of all contributions are computed.
2. Results outside the band $\mu^* \pm \sigma^*$ are considered outliers and discarded.
3. The reference value is computed as the mean μ of the remaining data. The ratio between the standard deviation of the remaining data and μ , μ/σ , is taken as an index to assess the spread of the valid contributions.

Figure 5 shows a plot of the flutter critical speeds predicted by different TG members for Step 1.1c, for a total of 12 contributions. Both statistics (with and without outliers) are shown. Contributions 2, 4 and 12 fall outside the spread band $\mu^* \pm \sigma^*$, and they are not considered in the computation of the reference value.

The reference flutter speed for Step 1.1c is therefore defined as $\mu = 72.31$ m/s, with a normalized standard deviation $\sigma/\mu = 0.42\%$. Step 1.1c differs from Step 1.1a, since by introducing the experimental flutter derivatives, the flutter speed results are more scattered with a normalized standard deviation 3.5 times larger than in the case with the flutter derivatives calculated with the theoretical Theodorsen functions (see Step 1.1a¹). This increase in the spread band is due to the introduction of the experimental coefficients, which are available only in the range $5 < V^* < 35$, instead of a fully defined analytical function.

Figures 6 and 7 report the natural frequencies and damping ratios of the unstable mode as a function of the mean wind speed. In these figures, a

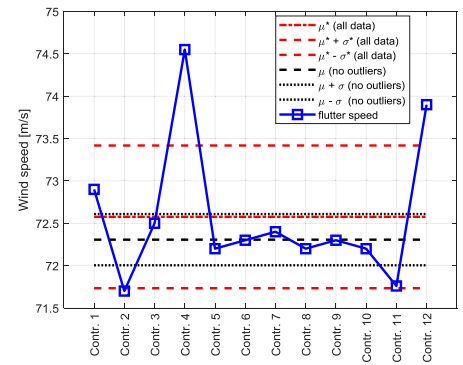


Fig. 5: Flutter critical wind speed results from different programs of the Task Group. Red lines: statistical values using all data; black lines: statistical values excluding outlier data

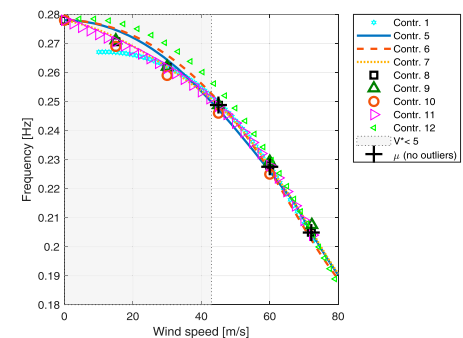


Fig. 6: Frequency of the unstable mode as a function of mean wind speed

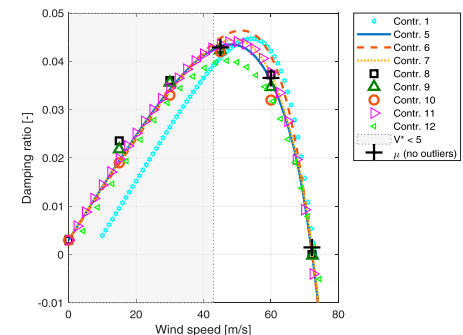


Fig. 7: Damping ratio of the unstable mode as a function of mean wind speed

vertical dashed line corresponding to $V^* = 5$ is also plotted, calculated using the torsional structural frequency reported in Table 1. For wind speeds lower than this value, the flutter derivative coefficients are not available and their values must be extrapolated. In current wind engineering practice, there are no standard rules for extrapolation: for high V^* , coefficients have an asymptote to the quasi-steady theory value that is used for extrapolation; for low V^* , no experimental information is generally available and therefore different approaches can be

used to model aeroelastic force in this region.

The discrepancy between numerical results is therefore also due to the method adopted to use the experimental coefficients, which are always provided in a limited range of V^* . One of the targets of this work is to highlight this kind of problem, and thus no rules are provided in the benchmark for extrapolation at low V^* ($V^* < 5$). For example, Contribution 1 does not connect to the structural eigenfrequency as an asymptotic value at $U = 0$ m/s (Fig. 6), and it also suggests a trend towards a negative structural damping at $U = 0$ m/s (Fig. 7): this is an index of incorrect extrapolation of the aerodynamic coefficients, and therefore these results for $V^* < 5$ should not be considered.

For $V^* > 5$, the frequency trends show a good agreement, while in the damping trend the largest differences are in the wind speed range between 45 and 65 m/s, where damping reaches its maximum value. These differences become smaller at larger wind speeds when the damping decreases.

Contributions 1 and 12 show discrepancies compared to the other damping trends, and the same contributions also differ in the flutter critical wind speed comparison. In contrast, Contribution 6 overestimates the damping ratio in the range between 45 and 65 m/s, with a flutter speed very close to the reference average value. As already highlighted in Ref. [1], considering only flutter speed is not sufficient to validate numerical codes, and the damping ratio trends versus the mean wind speed also have to be compared with reference data.

The reference μ or the frequency and damping ratio is reported in the plots as black markers, whereas the lines $\mu \pm \sigma$ are not shown for sake of simplicity; however, the normalized standard

		30 m/s	45 m/s	60 m/s	72 m/s
f_y [Hz]	μ	0520	0.0520	0.0520	0.0520
	σ/μ	01%	0.03%	0.04%	0.03%
f_z [Hz]	μ	1015	0.1029	0.1025	0.0933
	σ/μ	09%	0.26%	0.47%	0.62%
f_θ [Hz]	μ		0.2488	0.2275	0.2049
	σ/μ		0.36%	0.51%	0.41%

Table 3: Step 1.1c lateral, vertical and torsional frequencies: mean and standard deviation

		30 m/s	45 m/s	60 m/s	72 m/s
ξ_y [-]	μ	0122	0.0142	0.0169	0.0209
	σ/μ	63%	0.90%	1.42%	3.08%
ξ_z [-]	μ	0989	0.1660	0.2879	0.5099
	σ/μ	82%	2.03%	1.95%	5.94%
ξ_θ [-]	μ		0.0429	0.0366	0.0015
	σ/μ		1.69%	3.36%	97.9%

Table 4: Step 1.1c lateral, vertical and torsional damping ratios: mean and standard deviation

deviations σ/μ are listed in Tables 3 and 4. Contributions 6 and 12 fall outside the spread band at wind speeds equal to 45 and 60 m/s.

The reference values in the range $V^* < 5$ are discarded, since a reference extrapolation method is not defined by the TG 3.1 members and these results are not usable for the benchmark.

Buffeting Response Step 1.1c

The dynamic responses of the bridge due to the self-excited F_{se} and buffeting forces F_{buff} around the steady configuration of the bridge are compared.

The standard deviations of the lateral (y), vertical (z) and torsional displacement (z_{eq}) around the static position of the bridge (supposed to be equal to zero) versus the wind mean speed are presented in Figs. 8–10. The torsional values are expressed as equivalent displacement of the deck leading edge as $z_{eq} = (B/2)\theta$.

FD results are compared to TD results, where for TD approaches the plotted points are the average of the values of the ten time histories.

TD and FD results are presented together, but for a better understanding of the plots, FD values are shifted

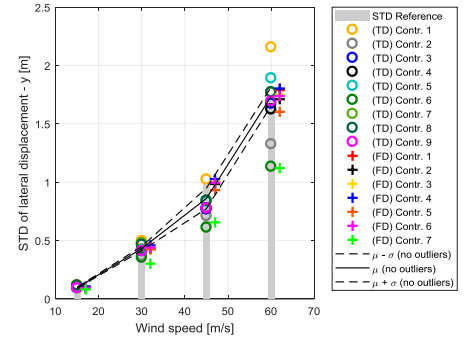


Fig. 8: Standard deviation (STD) of lateral displacement versus mean wind speed. TD, time domain; FD, frequency domain

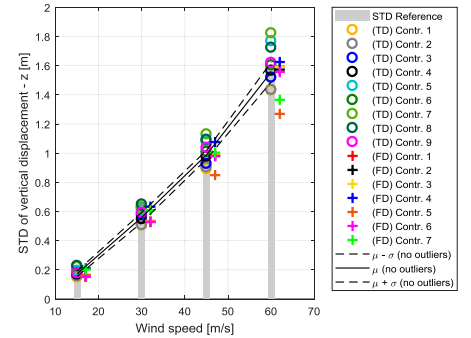


Fig. 9: Standard deviation (STD) of vertical displacement versus mean wind speed. TD, time domain; FD, frequency domain

by +1 m/s on the x -axis to prevent overlapping.

Figures 8–10 also report the statistical analysis of the results excluding outlier data ($\mu \pm \sigma$), using the methodology described in the previous subsection (“Aeroelastic Stability in Smooth Flow”). The average value μ is plotted with a solid black line, while the curves $\mu \pm \sigma$ are plotted with dashed black lines. In the next section (“Step 1.1c: Reference Values”), Table 5 displays the reference mean μ and the standard deviation ratio σ/μ

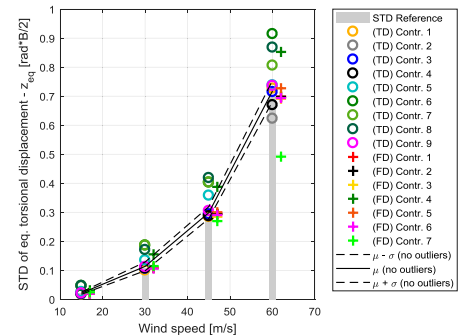


Fig. 10: Standard deviation (STD) of equivalent torsional displacement versus mean wind speed. TD, time domain; FD, frequency domain

		15 m/s	30 m/s	45 m/s	60 m/s
STD y	μ [m]	0.0952	0.4319	0.8616	1.7349
	σ/μ [-]	5.1%	4.1%	10.2%	4.6%
STD z	μ [m]	0.173	0.5596	0.9888	1.5557
	σ/μ [m]	10.5%	6.1%	3.0%	4.4%
STD z_{eq}	μ [m]	0.0211	0.1134	0.2984	0.7181
	σ/μ [-]	18.1%	13.2%	6.9%	5.0%

Table 5: Step 1.1c standard deviation (STD) of the lateral (y), vertical (z) and torsional displacement (z_{eq}): mean and standard deviation

computed excluding the outlier data at the five tested wind mean velocities, considering both TD and FD results, to allow validation against the reference data. Even excluding the outliers from the statistics, the standard deviation at 45 m/s reaches 3% on the vertical displacement, 7% on the torsional displacement and 10% on the lateral displacement. Considering the 16 contributions, the numbers of outliers for the four mean wind speeds (15, 30, 45 and 60 m/s) are as follows: for the lateral displacement 5, 4, 6 and 3; for the vertical displacement 7, 6, 7 and 5; and for the equivalent torsional displacement 3, 3, 5 and 5, respectively.

Figures 11–13 report the PSDs using the results of both the FD and TD analysis of lateral (y), vertical (z) and torsional equivalent displacement (z_{eq}) for a wind speed of 45 m/s. Only ten contributions in total are available, five in the FD and five in the TD. In both the vertical and the equivalent torsional displacements, three contributions are very far away from the others. STD values (STD_y , STD_z and $STD_{z_{eq}}$) computed by integration of the PSDs are reported in the key, for comparison with Figs. 8–10.

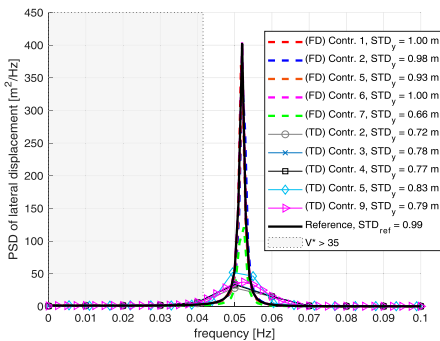


Fig. 11: Power spectral density (PSD) of lateral displacement, 45 m/s wind mean speed. FD, frequency domain; TD, time domain; STD, standard deviation

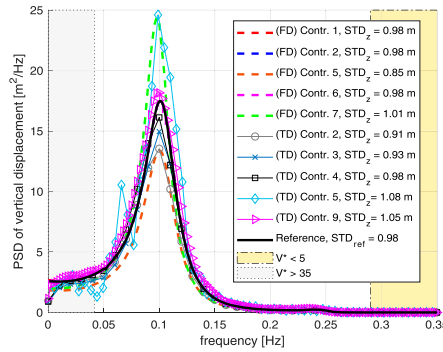


Fig. 12: Power spectral density (PSD) of vertical displacement, 45 m/s wind mean speed. FD, frequency domain; TD, time domain; STD, standard deviation

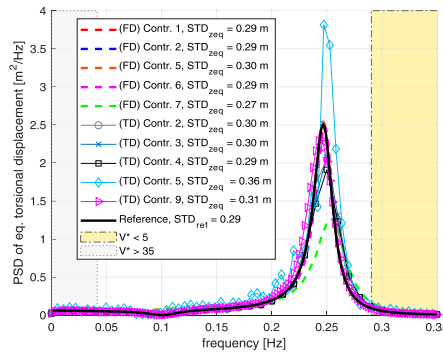


Fig. 13: Power spectral density (PSD) of equivalent torsional displacement, 45 m/s wind mean speed. FD, frequency domain; TD, time domain; STD, standard deviation

Considering that in Step 1.1c aerodynamic input data are defined in the FD, except for the extrapolation/interpolation against V^* , the different approaches in the FD should lead to the same results if the same extrapolation/interpolation method is used. In this case, instead of defining the statistical reference curve as the average of the collected results, a reference curve is directly computed, as reported in the Appendix, together with a numerical example of PSD computation in the FD, at 45 m/s, using a defined

extrapolation/interpolation method for aerodynamic coefficients (defined in the next section: “Step 1.1c: Reference Values”). The reference power spectra are also used to compute reference STD values (STD_{ref}) for comparison with the statistical average of the available results computed by the TG participants in the TD and FD. The reference STD values computed by integrating the reference power spectra are plotted in Figs. 8–10 as grey bars.

The reference values defined above are very close to the statistical values. This confirms that the procedure used in this paper to define the reference values μ , when analytical solutions are not available, is reliable thanks to the large number and good quality of most of the contributions, as presented in Ref. [1], where a fully analytical solution was available.

The STD trends (Figs. 8–10) clearly show that the absolute data spread increases with increasing wind speed, for both FD and TD approaches. However, the relative spread (σ/μ), reported in Table 5, is quite stable, highlighting the consistency of the independent analyses. This supports a validation procedure based on the comparison of results with an acceptance range defined through the trend of a reference value and a given tolerance.

Looking at Figs. 9 and 10, at 60 m/s, Contributions FD 5 and FD 7 are outliers. Comparing the corresponding PSDs in Figs. 12 and 13 at 45 m/s, it is clear that those models simulate a different aeroelastic behaviour from the others, as the PSD shape is very different from the others.

Moreover, considering 45 and 60 m/s, the TD approaches show a larger spread of STD compared to the FD approaches, and they underestimate STD mean values (excluding FD 5 and FD 7 values). To support this, by considering 60 m/s and separating the TD and FD results, it is possible to compare the σ/μ values of the different methodologies: σ/μ for lateral displacement is 17.9% for the TD and 4.1% for the FD approaches; for vertical displacement it is 8.7% and 8.6%, respectively; and for torsional displacement it is 12.2% and 8.7%, respectively.

Step 1.1c: Reference Values

This section summarizes the reference values presented in the previous sections.

f [Hz]	15 m/s	30 m/s	45 m/s	60 m/s
0.001	4.00E-02*	3.30E-01*	1.16E+00*	3.00E+00*
0.010	2.12E-02*	2.76E-01*	1.10E+00*	2.99E+00*
0.052	4.12E+00	8.88E+01	4.02E+02	1.01E+03*
0.100	7.00E-05*	2.70E-03	1.74E-02	6.09E-02
0.200	6.03E-07*	2.84E-05*	3.07E-04	3.95E-03
0.234	2.03E-07*	1.15E-05*	2.02E-04	2.53E-03
0.278	9.11E-08*	3.72E-06*	2.56E-05	8.00E-05
0.300	3.36E-08*	1.85E-06*	1.55E-05*	5.47E-05
0.350	1.09E-08*	6.55E-07*	5.92E-06*	2.47E-05

*Results obtained using extrapolated coefficients

Table 6: Step 1.1c power spectral density (PSD) of the lateral motion (reference values in $[m^2/Hz]$)

f [Hz]	15 m/s	30 m/s	45 m/s	60 m/s
0.001	6.36E-02*	5.89E-01*	2.58E+00*	9.43E+00*
0.010	6.05E-02*	5.75E-01*	2.55E+00*	9.35E+00*
0.052	6.64E-02	8.34E-01	3.56E+00	1.09E+01*
0.100	9.94E-01*	8.70E+00*	1.74E+01	2.47E+01
0.200	2.93E-04*	1.65E-02*	2.18E-01	2.46E+00
0.234	9.17E-05*	7.54E-03*	2.11E-01	1.92E+00
0.278	1.73E-05*	4.73E-04*	2.03E-03	4.23E-03
0.300	9.17E-06*	2.98E-04*	1.45E-03*	3.51E-03
0.350	3.41E-06*	1.64E-04*	1.08E-03*	3.28E-03

*Results obtained using extrapolated coefficients

Table 7: Step 1.1c power spectral density (PSD) of the vertical motion (reference values in $[m^2/Hz]$)

f [Hz]	15 m/s	30 m/s	45 m/s	60 m/s
0.001	1.52E-03*	1.40E-02*	6.12E-02*	2.21E-01*
0.010	1.38E-03*	1.33E-02*	5.91E-02*	2.15E-01*
0.052	8.59E-04	1.07E-02	4.50E-02	1.43E-01*
0.100	6.95E-05*	8.31E-05	2.94E-04	6.66E-04
0.200	2.86E-04*	1.60E-02*	1.95E-01	2.00E+00
0.234	5.35E-04*	4.26E-02*	1.11E+00	9.10E+00
0.278	1.16E-02*	9.19E-02*	1.89E-01	2.79E-01
0.300	5.03E-04*	1.40E-02*	5.54E-02*	1.15E-01
0.350	3.11E-05*	1.46E-03*	9.36E-03*	2.72E-02

*Results obtained using extrapolated coefficients

Table 8: Step 1.1c power spectral density (PSD) of the equivalent torsional motion (reference values in $[m^2/Hz]$)

In Table 3, the reference values of the natural frequencies of the system as a function of the mean wind speed are shown, while in Table 4 the reference values of the damping ratios are shown. Results of the lateral mode

(y), vertical mode (z) and torsional mode (θ) are reported at the five tested velocities as the reference mean μ and the ratio between the standard deviation σ and μ .

STD values of the buffeting response for the lateral (y), vertical (z) and the equivalent torsional (z_{eq}) displacements versus the wind mean speed for Step 1.1c are reported in Table 5. The STD values reported here are defined by the statistical average μ and by the normalized standard deviation σ/μ of the different contributions in both the TD and FD.

Tables 6–8 report the reference power spectra values defined in the previous subsection (“Buffeting Response Step 1.1c”) for the validation of numerical codes. Five frequencies are selected: the three resonant frequencies, a frequency before the first lateral mode and a frequency beyond the torsional mode. All five wind velocities are considered. The experimental flutter derivative values are defined in the range $5 < V^* < 35$, for a discrete set of V^* where every $\Delta V^* = 5$. Therefore, the values inside the range are interpolated with a linear method; the values outside the available range must be extrapolated. The results obtained using extrapolated coefficients are highlighted with an asterisk in Tables 6–8. Extrapolation is performed by keeping constant the experimental flutter derivative values outside the V^* range, considering the Polimi formulation presented in the subsection “Aerodynamic Forces”. Consequently, from 0 to 5 the values are kept equal to the data at $V^* = 5$, and from 35 to infinity equal to the data at $V^* = 35$.

Conclusions

IABSE TG 3.1 concluded successfully the second part of its working plan, the results of which are presented in this paper. For this step (Step 1.1c), TG 3.1 comprises a large and qualified number of participants, and the results represent the synthesis of many contributions. This aspect is very important, since one of the goals of TG 3.1 is the definition of reference data for the validation of numerical codes, and these reference data cannot usually be obtained through closed-form analytical approaches because of the complexity of the modelling.

Reference data were therefore defined according to a statistical analysis of the results provided by TG 3.1 participants, considering the average of the available data, preliminarily corrected for outliers. For the buffeting response computation in FD, where aerodynamic coefficients are experimentally defined, it is possible to define analytically the reference PSDs, having specified the interpolation method. These reference results are provided in the paper and compared to the statistical analysis of the results obtained by TG 3.1 participants, using different methods. The comparison highlights how the statistical post-processing of a wide and high-quality set of results allows for the definition of reliable reference data, supporting the adoption of this procedure in all the other benchmark steps.

Compared to Step 1.1a, Step 1.1c introduces the difficulty of the experimental aerodynamic coefficients, and includes the lateral degree of freedom and the horizontal turbulence wind component. Owing to the introduction of experimental coefficients, larger discrepancies are observed for the 3 DOF case. The TG 3.1 strategy of moving towards an increasing level of difficulty in the definition of numerical code validation turned out to be a correct procedure. If even a small level of complexity is added to the problem, differences from Step 1.1a arise.

In Fig. 5, for example, the standard deviation σ computed excluding the outlier data is 3.5 bigger than the case with the flutter derivatives calculated with the theoretical Theodorsen functions (as reported in Ref. [1]).

Furthermore, Step 1.1c shows a larger spread in the collected results for STD values before the statistical procedure to define the average value μ and standard deviation σ . Moreover, reference values are calculated with a different number of contributions with respect to Step 1.1a.

As highlighted in Ref. [1] and confirmed in Step 1.1c, the trend of the eigenvalues (frequency and damping) as functions of wind speed needs to be analysed together with the flutter wind speed for correct evaluation of the numerical models.

A similar conclusion is also valid for STD values in the buffeting response, since the STD value alone does not fully represent the quality of the modelling.

The results of Step 1.1c confirm that TD approaches show a larger dispersion of the output data, since different models of the aerodynamic forces are adopted with different approximations of the aerodynamic coefficients.

The next step of the benchmark will be Step 1.2, where the stability and the buffeting response of a numerical full-scale bridge will be studied. The dependency of experimental aerodynamic coefficients upon the angle on attack will be considered with a turbulent wind field defined in time and space (along the bridge axis).

To enhance the validation of the numerical codes, numerical results will also be compared against experimental results in Step 2, which is already in progress and the results of which will form part of a future publication.

Supplemental data

Supplemental data for this article can be accessed at <https://doi.org/10.1080/10168664.2019.1661331>.

Disclosure statement

No potential conflict of interest was reported by the authors.

ORCID

Tommaso Argentini  <http://orcid.org/0000-0003-0971-3659>

Miguel Cid Montoya  <http://orcid.org/0000-0002-3647-6022>

Ho-Kyung Kim  <http://orcid.org/0000-0002-1294-125X>

Daniele Rocchi  <http://orcid.org/0000-0002-5441-5979>

Appendix

At a given wind speed U , the equation of motion of the system in the frequency domain (FD) is (e.g. see Ref.

[29]):

$$\begin{aligned} & (-\omega^2[M_s + M_{se}(V^*)] \\ & + i\omega[R_s + R_{se}(V^*)] \\ & + [K_s + K_{se}(V^*)])X(f) = F_{buff}(f) \end{aligned} \quad (8)$$

where:

$$X(f) = \begin{Bmatrix} Y(f) \\ Z(f) \\ \Theta(f) \end{Bmatrix} = \mathfrak{F} \begin{Bmatrix} y(t) \\ z(t) \\ \theta(t) \end{Bmatrix}$$

is the vector of the Fourier transform of the free coordinates

- M_s, R_s, K_s are the 3×3 diagonal structural mass, damping and stiffness matrices

- M_{se}, R_{se}, K_{se} are the 3×3 self-excited mass, damping and stiffness matrices, written through flutter derivatives at a given reduced velocity V^*

$$F_{buff}(f) = \mathfrak{F} \begin{Bmatrix} F_{D,buff} \\ F_{L,buff} \\ M_{buff} \end{Bmatrix}$$

is the vector of the Fourier transform of the buffeting forces written through admittance functions at a given reduced velocity V^*

- $\omega = 2\pi f$ is the circular frequency.

The buffeting forces in the FD are defined through the Davenport function and the wind spectrum. Both are functions of reduced velocity V^* , so at a given wind speed U , they are functions of the frequency f . The Fourier transform of the vertical turbulent component $w(t)$ of the wind is $W_w(f)$, and that of the horizontal component $u(t)$ is $W_u(f)$. At a given wind speed U , the buffeting forces are defined in the FD as:

$$\begin{aligned} F_{buff}(f) &= \\ &= \left(\frac{1}{2} \rho U B \begin{bmatrix} \chi_{Du}^* & \chi_{Dw}^* \\ \chi_{Lu}^* & \chi_{Lw}^* \\ B\chi_{Mu}^* & B\chi_{Mw}^* \end{bmatrix} \right) \cdot \begin{Bmatrix} W_u(f) \\ W_w(f) \end{Bmatrix} \\ &= \chi_A(V^*) \cdot W_{uw}(f) \end{aligned} \quad (9)$$

Considering the above buffeting forces as an input, the output of the system in the FD is:

$$\begin{aligned} X(f) &= H(V^*)^{-1} F_{buff}(f) \\ &= H(V^*)^{-1} \chi_A(V^*) W_{uw}(f) \end{aligned} \quad (10)$$

where:

- $H(V^*) = (-\omega^2[M_s + M_{se}(V^*)] + i\omega[R_s + R_{se}(V^*)] + [K_s + K_{se}(V^*)])$ is the impedance matrix of the system at a given frequency f and reduced velocity V^* .

Taking the complex conjugate transpose of the complex output vector X :

$$\overline{X(f)} = \overline{W_w(f)} \overline{\chi_A(V^*)} \overline{H(V^*)}^{-1} \quad (11)$$

The cross-spectrum matrix of the output X will be:

$$X\overline{X} = H(V^*)^{-1} \chi_A(V^*) W_{uw}(f) \overline{W_{uw}(f)} \overline{\chi_A(V^*)} \overline{H(V^*)}^{-1} \quad (12)$$

where $W_{uw}(f) \overline{W_{uw}(f)}$ is the cross-spectrum of the wind turbulence.

The cross-power spectral density matrix $S_X(f)$ will be the expected value $E(X\overline{X})$ divided by $2\Delta f$, where Δf is the frequency resolution:

$$S_X(f) = H(V^*)^{-1} \chi_A(V^*) S_{wind}(f) \overline{\chi_A(V^*)} \overline{H(V^*)}^{-1} \quad (13)$$

where $S_X(f)$ is the cross-power spectrum matrix of the output, whose diagonal terms are the power spectral density (PSD) of the lateral motion S_y , of the vertical motion S_z and of the torsional motion S_θ . $S_{wind}(f)$ is the cross-power spectrum matrix of the incoming turbulence, defined as:

$$S_{wind}(f) = \begin{bmatrix} S_u & S_{uw} \\ S_{uw} & S_w \end{bmatrix} \quad (14)$$

the terms of which are defined in in [Table 2](#).

A numerical example of the PSD computation is reported to help the validation procedure.

Selecting a wind velocity U of 45 m/s and a frequency f of 0.278 Hz (the structural torsional frequency), the reduced velocity V^* is equal to 5.22 and the PSD of the wind $S_{wind}(f = 0.278)$ is:

$$S_{wind}(f) = \begin{bmatrix} 7.2139 & 0 \\ 0 & 5.2599 \end{bmatrix} \frac{(\text{m/s})^2}{\text{Hz}} \quad (15)$$

The admittance matrix $\chi_A(V^* = 5.22)$ is:

$$\chi_A(V^* = 5.22) = \begin{bmatrix} 0.0088 & 0.0116 \\ 0.0076 & 0.2536 \\ 0.0990 & 2.0687 \end{bmatrix} 10^4 \quad (16)$$

and the impedance matrix of the system at the given reduced velocity V^* is:

$$H(V^* = 5.22) = \begin{bmatrix} -6.74 + 0.11i & -0.01 + 0.01i & -0.29 - 0.26i \\ 0.07 + 0.04i & -6.25 + 0.80i & -19.40 - 0.37i \\ 0.06 + 0.23i & 0.50 + 5.39i & -158.52 + 79.71i \end{bmatrix} 10^4 \quad (17)$$

The cross-power spectrum matrix of the output $S_X(f = 0.278)$, through Eq. (13), is:

$$S_X(f = 0.278) = \begin{bmatrix} 0 - 0i & 1 + 1i & 1 - 1i \\ 1 - 1i & 20 - 0i & 0 - 13i \\ 1 + 1i & 0 + 13i & 8 - 0i \end{bmatrix} 10^{-4} \quad (18)$$

where the PSD of the lateral displacement is $S_y(f = 0.278) = 0.0$ (m²/Hz), the vertical displacement is $S_z(f = 0.278) = 0.0020$ (m²/Hz) and the PSD of the torsional displacement is $S_\theta(f = 0.278) = 0.0008$ (rad²/Hz). The torsional value expressed in equivalent displacement of the deck leading edge, according to $S_{z_{eq}}(f) = (B/2)^2 S_\theta(f)$, is equal to 0.1922 (m²/Hz).

By repeating the above example for all the desired frequencies f and wind speeds V , it is possible to obtain the PSD reference curves in the FD, as shown in [Figs. 11–13](#) for a wind speed of 45 m/s.

References

[1] Diana G, Stoyanoff S, Aas-Jakobsen K, Allsop A, Andersen M, Argentini T, Cid Montoya M, Hernández S, Jurado JÁ, Katsuchi H, Kavrov I, Kim HK, Larose G, Larsen A, Øiseth O, Omarini S, Rocchi D, Svendsen M, Wu T. IABSE Task Group 3.1 benchmark results. Part 1: Numerical analysis of a 2-degree-of-freedom bridge deck section based on analytical aerodynamics. *Struct. Eng. Int.* 2019. doi:10.1080/10168664.2019.1639480.

[2] Ding Q, Zhu L, Xiang H. Simulation of stationary Gaussian stochastic wind velocity field. *Wind. Struct.* 2006; 9: 231–243.

[3] Deodatis G. Simulation of ergodic multivariate stochastic processes. *J. Eng. Mech.* 1996; 122: 778–787.

[4] Diana G, Resta F, Zasso A, Belloli M, Rocchi D. Forced motion and free motion aeroelastic tests on a new concept dynamometric section model of the Messina suspension bridge. *J. Wind Eng. Ind. Aerodyn.* 2004; 92: 441–462.

[5] Argentini T, Pagani A, Rocchi D, Zasso A. Monte Carlo analysis of total damping and flutter speed of a long span bridge: effects of structural and aerodynamic uncertainties. *J. Wind Eng. Ind. Aerodyn.* 2014; 128: 90–104.

[6] Poulsen NK, Damsgaard A, Reinhold TA. Determination of flutter derivatives for the great belt bridge. *J. Wind Eng. Ind. Aerodyn.* 1992; 41: 153–164.

[7] Bucher CG, Lin YK. Stochastic stability of bridges considering coupled modes. *J. Eng. Mech.* 1988; 114: 2055–2071.

[8] Chen X, Matsumoto M, Kareem A. Time domain flutter and buffeting response analysis of bridges. *J. Eng. Mech.* 2000; 126: 7–16.

[9] Kavrov I, Morgenthal G. A comparative assessment of aerodynamic models for buffeting and flutter of long-span bridges. *Eng.* 2017; 3: 823–838.

[10] Garrick IE. *On Some Reciprocal Relations in the Theory of Nonstationary Flows*. NACA: Langley Field, VA, United States, 1938.

[11] Jain A, Jones NP, Scanlan RH. Coupled flutter and buffeting analysis of long-span bridges. *J. Struct. Eng.* 1996; 122: 716–725.

[12] Øiseth O, Sigbjörnsson R. An alternative analytical approach to prediction of flutter stability limits of cable supported bridges. *J. Sound Vib.* 2011; 330: 2784–2800.

[13] Øiseth O, Rönnquist A, Sigbjörnsson R. Finite element formulation of the self-excited forces for time-domain assessment of wind-induced dynamic response and flutter stability limit of cable-supported bridges. *Finite Elem. Anal. Des.* 2012; 50: 173–183.

[14] Øiseth O, Rönnquist A, Sigbjörnsson R. Simplified prediction of wind-induced response and stability limit of slender long-span suspension bridges based on modified quasi-steady theory: a case study. *J. Wind Eng. Ind. Aerodyn.* 2010; 98: 730–741.

[15] Øiseth O, Rönnquist A, Sigbjörnsson R. Time domain modeling of self-excited aerodynamic forces for cable-supported bridges: a comparative study. *Comput. Struct.* 2011; 89: 1306–1322.

[16] Shinozuka M. Monte Carlo solution of structural dynamics. *Comput. Struct.* 1972; 2: 855–874.

[17] Shinozuka M, Jan CM. Digital simulation of random processes and its applications. *J. Sound Vib.* 1972; 25: 111–128.

[18] Stoyanoff S. A unified approach for 3D stability and time domain response analysis with

- application of quasi-steady theory. *J. Wind Eng. Ind. Aerodyn.* 2001; **89**: 1591–1606.
- [19] Stoyanoff S. *Wind Induced Vibrations of Cable-Stayed Bridges*. K. University, A cura di, Japan; 1993.
- [20] Stoyanoff S, Dallaire PO. A Direct Method for Calculation of Wind Loads on Long-Span Bridges. *12th Americas Conference on Wind Engineering (12ACWE)*. American Association for Wind Engineering (AAWE); Seattle; 2013.
- [21] Park J, Jung K, Hong YH, Kim HK, Lee HS. Exact enforcement of the causality condition on the aerodynamic impulse response function using a truncated Fourier series. *J. Eng. Mech.* 2014; **140**(5): 04014017.
- [22] Jung K, Kim HK, Lee HS. Evaluation of impulse response functions for convolution integrals of aerodynamic forces by optimization with a penalty function. *J. Eng. Mech.* 2012; **138**: 519–529.
- [23] Jung K, Kim HK, Lee HS. New unified approach for aeroelastic analyses using approximate transfer functions of aerodynamic forces. *J. Eng. Mech.* 2014; **140**: 04013002.
- [24] Strømmen EN. *Theory of Bridge Aerodynamics*. Springer: Berlin, 2010.
- [25] Matsumoto M, Okubo K, Ito Y, Matsumiya H, Kim G. The complex branch characteristics of coupled flutter. *J. Wind Eng. Ind. Aerodyn.* 2008; **96**: 1843–1855.
- [26] Høgsberg JR, Krabbenhøft J, Krenk S. State space representation of bridge deck aeroelasticity. In *13th Nordic Seminar on Computational Mechanics - NSCM13*, Hellelands J, Osnes H, Skeie G (eds). University of Oslo: Oslo, 2000, pp. 109–112.
- [27] Diana G, Rocchi D, Argentini T. An experimental validation of a band superposition model of the aerodynamic forces acting on multi-box deck sections. *J. Wind Eng. Ind. Aerodyn.* 2013; **113**: 40–58.
- [28] Diana G, Rocchi D, Argentini T. *Buffeting Response of Long Span Bridges: Numerical-Experimental Validation of Fluid-Structure Interaction Models*. International Association for Bridge and Structural Engineering (IABSE); Geneva; 2015.
- [29] Scanlan RH. On flutter and buffeting mechanisms in long-span bridges. In *Lecture Notes in Engineering*. Springer: Berlin, 1987; 371–387.